GPS Solutions (2024) 28:147
https://doi.org/10.1007/s10291-024-01684-w

ORIGINAL ARTICLE

# LSTM-based clock synchronization for satellite systems using inter-satellite ranging measurements

**Xiaobo Gu[1] · Zeyang Qiu[2] · Yanjiao Wang[2] · Wei Jiang[3]**

Received: 21 February 2024 / Accepted: 28 May 2024 / Published online: 23 June 2024
© The Author(s), under exclusive licence to Springer-Verlag GmbH Germany, part of Springer Nature 2024

**Abstract**
The inter-satellite link (ISL) has been received increasing attention, as it is a potential way to achieve autonomous clock synchronization for envisioned space-based satellite networks with minimal ground segment capability. Existing satellite clock synchronization solutions either rely on prior information or modelling the relative motion by an approximated polynomial. In this paper, we propose a deep learning approach based on long short-term memory (LSTM) to decouple the clock parameters from pseudo-range measurements. The process of clock parameter estimation solely relies on the observed pseudo-range measurements, and the prior information of position and velocity are not required and the nonlinear relative motion process is modelled by training on historical data. The simulation results show that the proposed method outperforms the benchmark solutions in terms of accuracy.

**Keywords** Clock synchronization · LSTM · Inter-satellite link · Two-way ranging

## Introduction

### Background

As the development of integrated electronic technology and the growing demand, the number of on-board satellites has experienced explosive growth during the last decades. Satellite networks, as opposed to individual large spacecraft, offer a myriad of benefits, including abbreviated development cycles, diminished launch expenses and enhanced maneuverability. The collaborative network formed by multiple satellites enhances adaptability, scalability, reliability, invulnerability and reconfigurability of the system.

When satellite systems perform tasks such as relative positioning (Kai et al. 2013), orbit determination (Ruan et al. 2020; Xie et al. 2020) and earth observation (Michalak et al. 2021), achieving high accuracy clock synchronization between each satellite is the fundamental premise, and the requirements for time synchronization in these cutting-edge scientific fields are still increasing. It should be noted that factors including volume, weight and power consumption are critical as they determine the overall launch cost of space missions. In order to reduce the overall cost and make full use of the existing resources, satellite systems normally require the fundamental temporal-spatial information provided by external system to maintain the system function. These high-cost infrastructures can provide high-accuracy position, navigation and timing (PNT) services. Moreover, the cost for users to obtain these services is very low. In general, satellite clock synchronization requires external assistance from ground stations (Iwata et al. 2010; Fujieda et al. 2014) or global navigation satellite system (GNSS) (Glennon et al. 2013). However, such a design is not feasible for the inaccessible scenarios such as deep space. Moreover, relying on ground station assistance requires the use of a large number of ground-based relay systems and global tracking systems, which takes up a considerable amount of manpower and material resources. In addition, for satellite networks used for military purposes, if ground stations or

✉ Yanjiao Wang
yjwang12@gdut.edu.cn

✉ Wei Jiang
weijiang@bjtu.edu.cn

[1] School of Integrated Circuits, Guangdong University of Technology, Guangzhou, China

[2] School of Automation, Guangdong University of Technology, Guangzhou, China

[3] School of Electronic and Information Engineering, Beijing Jiaotong University, Beijing, China

GNSS satellites are destroyed during wartime, the satellite systems that do not have the ability to operate autonomously would be paralyzed.

To achieve clock synchronization, a reference clock frame must be selected. For low earth orbit (LEO) satellites, especially CubeSats which have strict restriction on overall cost, the GNSS signals are implemented as the reference to perform on-board clock steering (Glennon et al. 2013; Meng et al. 2020). However, such a method is vulnerable since it relies on the external system and the timing service of GNSS has limited accuracy (about 20 ns). Although the Galieo is developing a new timing service whose highest timing accuracy reaches 5 ns (Fernandez-Hernandez et al. 2022), it still cannot meet the requirement of some particular missions. Take the time-of-arrival (TOA) ranging techniques for example, nanosecond level clock synchronization performance could lead to centimeter-level ranging error. If the GNSS signal is unavailable, the clock synchronization accuracy of the CubeSats would decrease, as the clock reference source turns to the on-board clock in this case and the stability of the on-board clock is limited. If one of the system member is chosen as the reference and broadcasts its timing information, then the other members are able to be synchronized to it remotely (Powers and Colina 2016). Such a one-way time transfer mechanism requires the accurate position information so that the clock deviation can be decoupled form the TOA measurements. In order to solve this problem, the two-way ranging (TWR) technique (Karthik and Blum 2020; Domuta and Palade 2021; X. Gu et al. 2021) is presented to jointly estimate the clock parameters and relative distance. In comparison to one-way ranging, TWR is capable of achieving higher estimation accuracy and estimating the clock parameters under unknown relative distance. However, the positions of nodes must be fixed during the TWR process, so that the relative distance of the forward link equals to that of the reverse link. On the other hand, since the satellites are in high dynamic motion, whose effect on TWR-based clock synchronization must be taken into account. In this case, the signal propagation delays of the forward link and the reverse link are not equal, and thus the number of unknown ranging parameters increases. In addition, the signal propagation delay becomes a time varying parameter due to relative motion.

All these facts reveals that the problem of constructing a full column rank matrix to perform estimation based on statistical signal processing needs to be addressed. The prior information provided by the ephemeris can be used to decouple the clock parameters from the pseudo-range measurements, namely, the positions and velocities of the satellites are implemented to calculate the signal propagation delay so that the number of unknown parameters can be reduced to meet the requirement of full column rank (Kim and Tapley 2003; Xu et al. 2012; Xiaobo Gu et al. 2015). However, in scenarios involving the ISL where communication between ground stations and satellites is unavailable, it becomes imperative to explore clock bias estimation by leveraging satellite velocity, position, and pseudo-range information. The estimation accuracy strongly relies on this information, and thus the absence of certain information might significantly degrade the accuracy.

In recent years, researchers have been working on methods to achieve clock synchronization by relying solely on ranging information without the assistance of prior information. In (Rajan and Veen, 2015), a least square (LS) method is presented which requires a number of rounds of TWR measurements to jointly estimate the parameters of ranging and clock for nano-satellites, and it is able to perform estimation only by exchanged timing tags. A step further, a LS estimator based on pseudo-range measurements is proposed in (X. Gu et al. 2020), which reduces the communication load by utilizing the synchronous two-way ranging (STWR) technique. Moreover, to reduce the computation complexity and apply off-line computation, the iterative estimators such as Kalman filter (KF) are proposed (X. Gu et al. 2021). In theory, the performances of these statistical signal processing approaches rely on the proposed kinetic model, which aims to adopt a polynomial to characterize the relative motion model over a short period of time. In addition, a number of approximations are required to reduce the dimension of information matrix to get a unique solution. However, the relative kinetic model for satellite networks is complicated and varies over time, which makes it difficult to be expressed as a linear function with respect to time. Therefore, how to accurately model the non-linear relative motion process becomes a challenging work which determines the performance of clock synchronization.

Due to the excellent performance in nonlinear parameter estimation, the machine learning (ML) and deep learning (DL) approaches have been adopted to estimate the states of satellite networks. In data-driven solution scenarios, methods based on ML and DL can exploit data features to uncover abstract relationships between data. The satellite orbit prediction, which is a nonlinear function with respect to time, is a applicable scenario for ML methods (Haidar-Ahmad et al. 2022). On the other hand, clock parameters estimation can also be estimated, as the clock parameters are coupled with the nonlinear ranging parameters. Most existing studies involve modeling clock bias data provided by precision data service centers such as the international GNSS service (IGS) data center to forecast clock bias data for a period of time (Huang et al. 2021). This process encompasses various data analysis methods based on ML and DL. A wavelet neural network (WNN) model based on the single difference sequence of satellite clock bias is proposed to predict the next single difference values (Wang et al. 2017). In (Ya et al.

2022), an improved BP neural network based on the beetle swarm optimization (BSO-BP) algorithm is presented to solve the local optimum problem of BP neural network, and the experimental results in third-generation Beidou satellite navigation system (BDS-3) perform its validity in terms of accuracy. In (Huang et al. 2021) and (He et al. 2023), the authors established a satellite clock bias prediction model based on long short-term memory (LSTM) that can accurately express the nonlinear characteristic of satellite clock bias after preprocessing the outliers in the original clock bias. These methods aim to address the challenge of maintaining satellite clock bias data even in the event of interruptions in the real-time satellite observation data stream. Accordingly, it appears to be reasonable to use artificial neural networks (ANNs) to solve the problem of the satellite clock bias prediction (Wang et al. 2017). However, the complexity of atomic clock can lead to limitations in the accuracy of clock bias predictions.

The DL model has an outstanding advantage that it can be trained to fit a function that matches the distribution of the values by adjusting the weights. The existence of relational transformations between satellite information makes it possible to use satellite pseudo-range, velocity, position and other information to estimate the satellite clock bias. The input data required for the model in a time-series prediction problem is usually in the form of feature data and the corresponding result data. The internal operation of the neural network is to use the feedback error to minimize the loss function while continuously learning and updating the model parameters through forward and backward propagation, resulting in a functional mapping between the feature data and the result.

In recent years, the application of deep-learning models has gained significant traction in time series analysis. Particularly, the advent of recurrent neural networks (RNNs) has revolutionized the field by incorporating the temporal dimension into traditional neural networks, allowing for the establishment of temporal relationships within the data. However, as the time span of the analyzed sequence increases, RNNs models encounter challenges such as vanishing gradients and gradient decent issues during the back-propagation process. To mitigate these challenges, the LSTM variant of RNNs has been developed (Lipton 2015). The LSTM architecture consists of three gates, and all of them employ the sigmoid activation function. This choice ensures that the gate outputs are confined to values close to either 0 or 1. Outputs approaching 1 facilitate the effective propagation of gradients, while outputs close to 0 indicated that the information from the preceding time step has negligible influence on the current time step, thereby eliminating the necessity of propagating gradients to update the model parameters.

## Potential applications

Our motivation for this work is to enable the satellite network to achieve clock synchronization as accurate as possible, with the absence of time, distance and position information from any external system. The pseudo-ranges among the satellite members are the only observable parameters to carry out clock synchronization. Different from the existing methods, the proposed estimator gets rid of the process of linearizing the complex relative motion model, and free the constraint of relying on prior information. Therefore, the proposed method can be applied in other networks of self-organized, complex moving trajectory and limited prior information, such as unmanned aerial vehicle swarm, robot system, cooperative man-unmanned system, indoor positioning and deep space aircraft.

## Contributions

The main contributions of this paper compared with the existing TWR-based clock synchronization literature are three folds.

1. We introduce a clock synchronization framework based on STWR. Unlike the traditional timing stamps exchanged mechanism, only a pair of pseudo-range measurements are exchanged for each communication cycle to perform parameter estimation.
2. A LSTM-based parameter estimation method is derived to model the nonlinear relative motion process, which is able to estimate the clock bias using previously observed pseudo-range measurements based on relative kinematics. Additionally, compared with the existing approaches, the information of velocity and position are no longer required.
3. We evaluate the performance of the proposed method and benchmark solutions using the satellite orbit data generated by the satellite tool kit (STK), the results show that the proposed estimator outperforms the benchmark solutions in terms of clock synchronization accuracy.

The rest of this paper is organized as follows. The basic ranging model and clock model are introduced in Sec. "System model". We conclude by comparing the proposed approach (outlined in Sec. "Proposed estimator" and Sec. "Parameter selection") to existing methods in Sec. "Case studies".

## System model

### Clock *bias* model

We consider a network structured in a master/slave architecture. In such a setup, there exists a central entity known as the master satellite, which serves as the reference satellite for coordination and calibration. Thus, the on-board clock of the master satellite is assumed to be perfectly stable and accurate, while multiple slave satellites communicate with it directly by way of the ISLs. As synchronous time division duplex (STDD) is adopted in this study, that ensure the consistent states among all the transceivers. In theory, it has been demonstrated that the accuracy of the STWR technology under the STDD communication framework surpasses that of polling time division duplex (PTDD) scheme (Xu et al. 2012).

The clock bias model can be expressed as:

$$x(t) = a_0 + a_1 t + \frac{1}{2} a_2 t^2 + \psi(t) \tag{1}$$

where the coefficients $a_0$ signifies an initial clock offset between the local clock and the reference clock, which is denoted as the phase deviation; $a_1$ represents the frequency deviation, and $a_2$ the fractional frequency drift rate, denoted as frequency drift (Allan et al. 1972), while $\psi(t)$ denotes the aggregated phase noise, which can be expressed as a linear superposition sum of five independent noises, and the power-law spectral density expression is given by

$$\begin{aligned} S_y(f) &= h_{-2} f^{-2} + h_{-1} f^{-1} + h_0 f^0 + h_1 f^1 + h_2 f^2 \\ &= \sum_{\alpha=-2}^{2} h_\alpha f^\alpha, \end{aligned} \tag{2}$$

where the random noise terms are known in the metrological literature as.

$\alpha = -2$: random walk frequency modulation (RWFM).
$\alpha = -1$: flicker frequency modulation (FFM).
$\alpha = 0$: white frequency modulation (WFM).
$\alpha = 1$: flicker phase modulation (FPM).
$\alpha = 2$: white phase modulation (WPM).

### STWR

In general, to achieve clock synchronization, one satellite is designated as the master satellite, and the others are called slave satellites. The onboard clock of the master satellite is designated as the reference clock, so there is a clock offset between the master satellite and the slave satellites. It is possible to compensate for this difference by estimating the clock bias, thus reducing the effect of the clock deviation and then achieving clock synchronization. Although it is possible to extend the pairwise mode to a star topology that includes one master satellite and a plurality of slave satellites, this study only focuses on a master–slave structure involving twin satellites for the sake of description.

At the initiation of the specified global transmission slot, the communication state of each satellite switches into signal transmission mode and dispatches the information frame with the analogous structure. These frames encapsulate the local pseudo-range measurements derived from the last communication round. Due to the fact that the local clock of the satellite is generated independently from the local frequency synthesizer, there must be a time difference between the local time and the global time. The satellites receive the signal at the commencement of the reception time slot. Subsequent processes include the acquisition, tracking and demodulation of these signals to recover the original signal.

Assuming constant visibility and uninterrupted communication between the two satellites, both the master and slave satellites are required to simultaneously transmit ranging signals to each other per $\delta$ seconds. The system operation period is divided into a number of identical frames, which are composed of several time slots. The satellites execute a round of signal transmission and reception operation within a time slot, and repeat this operation continuously. All the satellites are required to simultaneously transmit signals to other satellites at the beginning of the transmission slot and switch to the receiving mode at the beginning of receiving slot (Xu et al. 2012). We define the duration of each time frame as the time interval $\delta$ for each round of inter-satellite communication. However, due to the presence of clock bias between the satellites, the actual transmission times of the two satellites are not identical. Figure 1 illustrates the principle of STWR measurement. Notably, we designate the signal transmission time of the master satellite as the reference time for each round of two-way communication. For the $i^{th}$ round of STWR, the clock bias $\Delta t^i$ between slave satellite $B$ and master satellite $A$ can be deduced by

$$\Delta t^i = t_B^i - t_A^i \tag{3}$$

As the signal transmitted by the master satellite propagates through space and then receipt by the slave satellite, a number of delays occur during the whole process. Therefore, the pseudo-range measurements consist of the signal transaction time, clock bias and other delays, which can be expressed as

$$\begin{cases} \rho_{AB}\left(t_A^i\right)/c = \tau_{AB}\left(t_A^i\right) - \Delta t^i + Z_{AB} + I_{AB} + \varepsilon_{\tau A} \\ \rho_{BA}\left(t_B^i\right)/c = \tau_{BA}\left(t_B^i\right) + \Delta t^i + Z_{BA} + I_{BA} + \varepsilon_{\tau B} \end{cases} \tag{4}$$

where $\tau_{AB}(t_A^i)/\tau_{BA}(t_B^i)$ denotes the signal propagation delay from $A/B$ to $B/A$, $Z_{AB}/Z_{BA}$ denotes the unidirectional

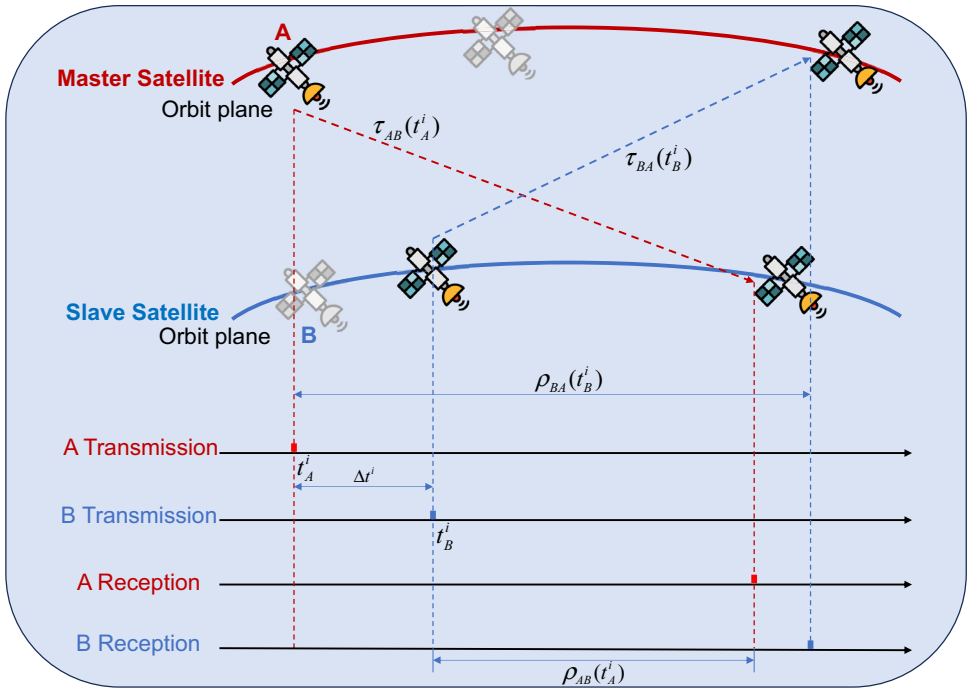


**Fig. 1** The schematic diagram of STWR during the $i$ th round of signal transactions, satellite A is selected as the master

combined device delays from $A/B$ to $B/A$, $I_{AB}/I_{BA}$ denotes the ionospheric delay of the signal from $A/B$ to $B/A$. $\varepsilon_{\tau A}$ and $\varepsilon_{\tau B}$ denote the measurement noise. It should be noted that the error sources including device delay, ionospheric delay and other delays can be ignored or be compensated by the corresponding solutions, as discussed in (Xu et al. 2012; Xiaobo Gu et al. 2015). The aggregated residual errors are assumed to be Gaussian components with zero mean. Therefore, after the open-loop clock bias compensation process, the pseudo-range measurements $\rho$ in Eq. (4) consist of signal propagation time $\tau$, clock bias $\Delta t$ and residual error. If the ephemeris data can be utilized, the signal propagation time $\tau$ can be calculated as the positions and velocities of the satellites are known, and then the clock bias can be decoupled from $\rho$. In order to remove reliance on the prior information, we aim to estimate the clock bias solely based on pseudo-range measurements in this paper.

## Proposed estimator

Based on the discussions above, we can infer that the key is how to decouple the clock bias from the observed pseudo-range measurements. According to Sect. "Introduction", the existing solutions either utilize the velocity and position information to directly calculate the signal propagation time, or jointly estimate the clock and range parameters based on statistical signal processing algorithm. Although the latter is able to achieve clock synchronization with the absence of the prior information, the complex relative motion is difficult to be modelled by the Taylor series with respect to the reference time. Moreover, determining the order of the Taylor series is also difficult owing to the time varying relative motion.

Although the pseudo-range is the only observable measurement, a series of pseudo-range measurements over a period of time comprises the statistical correlation in clock bias and relative motion. In light of this investigation, a LSTM-based clock bias prediction framework is proposed to improve the estimation accuracy.

In the RNN system, the state of the hidden layer combines the current input information and the previous hidden layer state. This tight coupling between the readout signal at one step and the state signal at the next step directly impacts the gradient of the objective function with respect to the state signal (Sherstinsky 2020). The gradient is propagated through the time steps, using the chain rule to calculate the gradient at each time step. The problem arises in long sequences where gradients can become very small or very large, making parameter updates unstable. LSTM addresses the vanishing gradient problem by introducing a gating mechanism. The key components in LSTM structure are the input gate, forget gate and output gate, which regulate information flow. The forget gate allows the network to selectively remember or forget information, preventing the vanishing gradient by controlling the flow of gradients through time.

Figure 2 shows the time series processing diagram of LSTM, which has showcased capabilities in demonstrating a high level of sensitivity toward temporal patterns. This neural

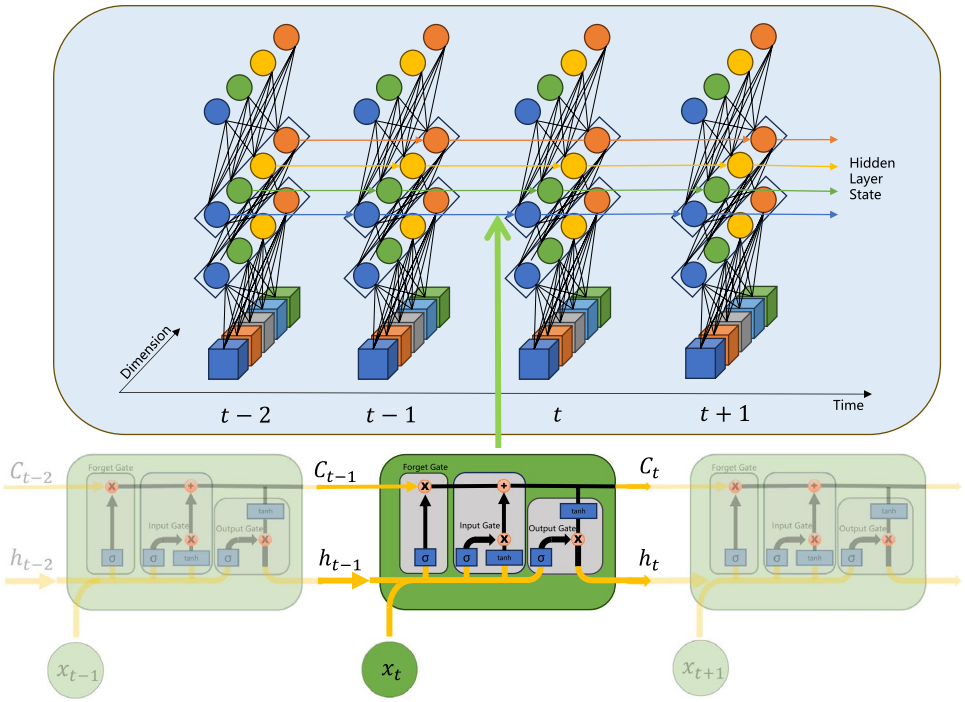


**Fig. 2** LSTM neural network structure

network architecture is the advancement of the RNN, which introduces the concept of cell states, enabling the model to retain information about prior predictions. Through the manipulation of these cell states, LSTM effectively addresses the issue of vanishing gradients inherent to RNN, thus compensating for their deficiency in long-term memory retentio.

As shown in Fig. 2, the LSTM nodes are defined as follows:

$$g_t = \phi\left(W_{gx} * x_t + W_{gh} * h_{t-1} + b_g\right) \tag{5}$$

$$i_t = \sigma\left(W_{ix} * x_t + W_{ih} * h_{t-1} + b_i\right) \tag{6}$$

$$f_t = \sigma\left(W_{fx} * x_t + W_{fh} * h_{t-1} + b_f\right) \tag{7}$$

$$o_t = \sigma\left(W_{ox} * x_t + W_{oh} * h_{t-1} + b_o\right) \tag{8}$$

$$C_t = g_t * i_t + C_{t-1} * f_t \tag{9}$$

$$h_t = \phi\left(C_t\right) * o_t \tag{10}$$

where the functions $\sigma(\cdot)$ and $\phi(\cdot)$ are given by

$$\sigma(\theta) = \frac{1}{1+e^{-\theta}} \tag{11}$$

$$\phi(\theta) = \frac{e^{\theta} - e^{-\theta}}{e^{\theta} + e^{-\theta}} \tag{12}$$

$x_t$ denotes the current moment, while $h_{t-1}$ is the hidden state from the last moment. $W_*$ and $b_*$ are the weight matrix and bias, respectively. $\sigma$ and $\phi$ denote the sigmoid activation function and tanh activation function. $C_t$ denotes the cell state of LSTM. The data processing of LSTM involves three internally designed gates: Input Gate, Forget Gate and Output Gate. In Eq. (7), the current input and hidden layer state of the previous state are multiplied by weight matrices $W_{fx} \in \mathbb{R}^{d_h \times d_x}$ and $W_{fh} \in \mathbb{R}^{d_h \times d_h}$, where $d_x$ and $d_h$ denote dimension of the input data and the hidden layer state, respectively. After passing through a sigmoid function to map the value from 0 to 1, this processing can determine what information to discard from the previous state of cell. In Eq. (6) and Eq. (9), the input gate incorporates the data that has already been processed by the Forgot Gate to update the current state of the cell. The Output Gate is responsible for passing the updated cell state to the next cell, passing the current cell state through tanh function and merging it with $x_t$ and $h_{t-1}$ to update the hidden layer state $h_t$.

Unlike specialized time series models focusing solely on satellite clock bias data, our proposed model harnesses historical pseudo-range data to forecast satellite clock bias variations over an extended future timestamp, ensuring a certain degree of estimation accuracy. This approach stands apart from typical regression problems, as we utilize the time series of pseudo-range data, with clock bias data between satellites as the output, which preserves the continuity characteristics of the data in the time dimension.

While intuitively satellite clock bias data and pseudo-range data might not exhibit direct correlations and do not directly derive from each other, which contains the effect of complex relative motion. Thus, the analyzing these time series data through LSTM enables the establishment of internal patterns and trends between them.

In the majority of satellite clock bias prediction studies, many scholars employ the precise clock bias data obtained from ground stations. They segment such data using differencing operations and sliding windows, generating new time series data characterized by fixed time steps. The goal of prediction is the satellite clock bias data for a future time period. Although LSTM offers training modes for multi-step and single-step predictions, current prediction values must be restructured as ground truth data for the next step prediction due to the inherent structure of model's input and output. This unavoidably leads to an accumulation of prediction errors. However, the proposed training approach circumvents this drawback, which requires the proper functioning of signal transmission and reception so that the corresponding pseudo-ranging measurements can be collected. This data prediction methodology always takes pseudo-range measurements as model input, effectively mitigates the accumulation of errors.

Figures 3 and 4 shows the process of data processing and sequence construction. The above aspects need to be improved as following steps:

Step 1. In the context of pseudo-range data of each round of signal transactions from the master satellite and slave satellite, we form them into two-dimensional vectors and convert this time sequence into a multi-feature variable using an equidistant interval, representing multiple time steps. For the whole-time sequence $\mathcal{X} = \{X_1, X_2, X_3, ..., X_N\}$ is the data of a known pseudo-range sequence of satellite-link. We use the window size as the time-steps for pseudo-range data. By rolling this window, we reconstruct the data into multiple segments and reassemble the segments to new time sequences. The time-step dimension $p$ through the way of equidistant interval satisfies $p \ll N$. Then, it produces a new pseudo-range sequence:

$$\begin{bmatrix} \{X_1, X_2, X_3, \dots, X_{p-1}, X_p\} \\ \{X_2, X_3, X_4, \dots, X_p, X_{p+1}\} \\ \dots \\ \{X_{N-p+1}, X_{N-p+2}, X_{N-p+3}, \dots, X_{N-1}, X_N\} \end{bmatrix} \tag{13}$$

Step 2. We employ a training approach within the LSTM model whose format is multi-input and single-output, essentially constituting supervised learning problem. We regard the clock bias data $\mathcal{Y} = \{Y_1, Y_2, Y_3, ..., Y_{N-1}, Y_N\}$ as target values. Commencing from the $p^{th}$ clock bias data point, we obtain a new sequence of clock bias: $\{Y_p, Y_{p+1}, ..., Y_N\}$ using the same sliding distance as described in Step 1.

Step 3. In the context of Step 1 and Step 2, a new data set is established to capture the relationship between pseudo-ranges and clock bias. Their correspondence is defined such that each segment of fixed time-step pseudo-range values corresponds to the clock bias value at the final moment:

$$\begin{bmatrix} \{X_1, X_2, X_3, \dots, X_{p-1}, X_p, Y_p\} \\ \{X_2, X_3, X_4, \dots, X_p, X_{p+1}, Y_{p+1}\} \\ \dots \\ \{X_{N-p+1}, X_{N-p+2}, X_{N-p+3}, \dots, X_{N-1}, X_N, Y_N\} \end{bmatrix} \tag{14}$$

Step 4. All data need to be normalized firstly, as this process can enhance the accuracy and speed of model convergence. In the final step of clock bias prediction, it is necessary to perform inverse normalization to revert it to its original scale, ensuring the integrity of information.

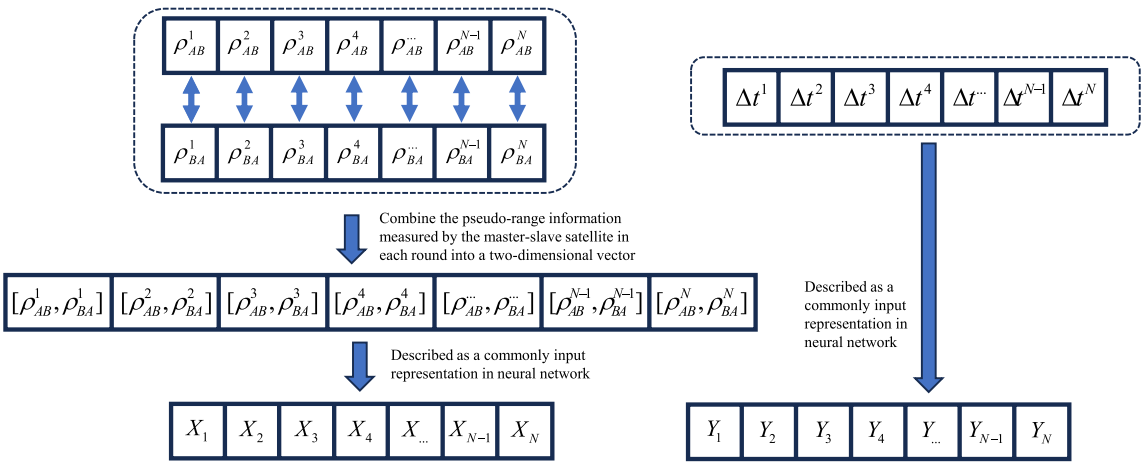


**Fig. 3** Process of rearranging the pseudo-range measurement values obtained from each round of STWR to input vectors

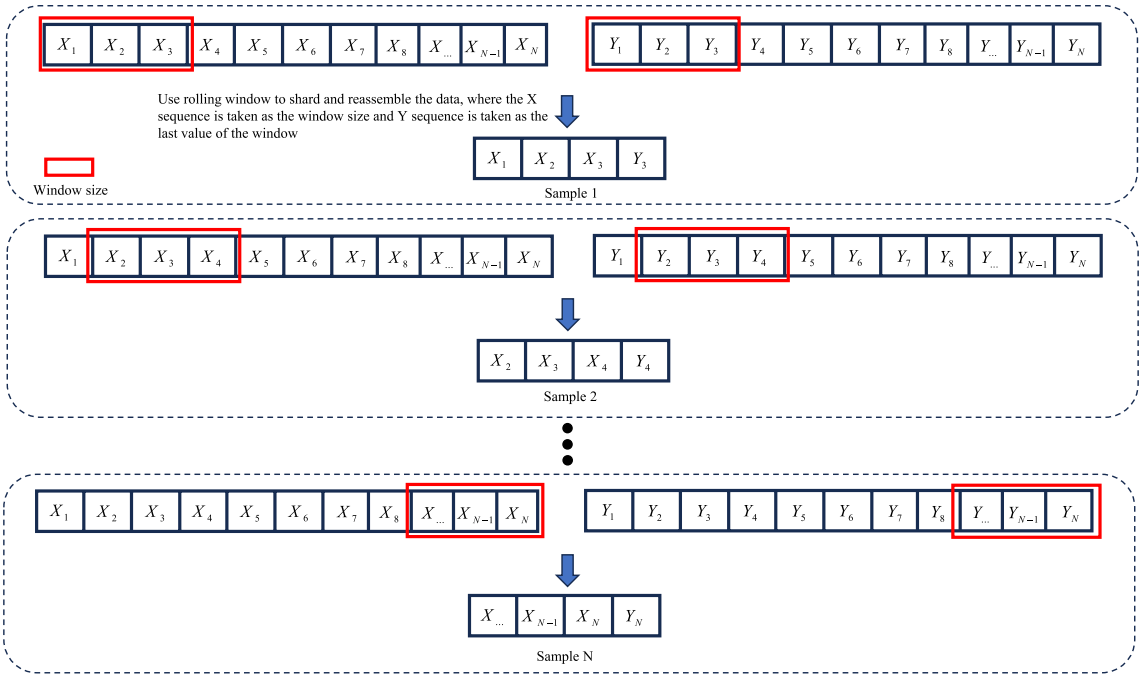


**Fig. 4** Process of constructing multi-variable sequence

We establish a mapping relationship between the sequence of pseudo-range and clock bias. This approach involves mining the trends in clock bias in a data-driven way. It is different from the multi-step prediction approaches based on the clock bias, which regard the predicted value as a new observation to further extrapolate future periods. The shortcomings of the multi-step predicting method have been discussed in (He et al. 2023). When the multi-step predicting method is implemented to predict the clock bias for a long period of time, the previously obtained prediction must be used as the input of the model. It is worth noting that such a process will lead to the gradual accumulation of model errors over time. In order to solve this problem, we transform the time series prediction problem of clock bias into regression problem. We let the observed pseudo-range measurements of each communication cycle be features, as they are more reliable and accurate than the clock bias prediction value in the "clock bias"-based approaches using multi-step prediction. This effectively mitigates the issue of error accumulation during long-term predictions, resulting in increased precision and reliability. Additionally, it offers a degree of interpretability. The detailed procedure of data processing is illustrated in Fig. 5.

## Parameter selection

The method we propose is based on a neural network model rooted in the fundamental principles of LSTM networks, constructed using the Keras deep-learning framework. Neural network parameters play a significant role in determining the performance and efficiency of the model. In time series problems, data is typically structured in a three-dimensional format, requiring the shape (samples, time-step, features). The choice of the time-step length varies across different scenarios of time prediction problems. In cases with limited data samples, the time-step length may be constrained by the small data set size. Our original data consists of satellite-related information collected at sampling frequencies of 5 Hz and 1 Hz, allowing for the selection of relatively larger time-step lengths to capture temporal correlations. However, the determination of the time-step length is considered a hyper-parameter in neural network modeling and necessitates extensive experimentation to find an appropriate length tailored to the specific data set and its nonlinear temporal features between pseudo-range and clock bias.

Theoretically, limited time-step length makes the model difficult to capture temporal relationships in data changes trend, while larger time-step length can obtain higher accuracy but result in the cost of increased computational complexity. Therefore, the chosen of time-step length should be taken into account. The details of the final specific parameters we set are listed in Table 1. The pseudo-range data and clock bias data in a day have a total of 86,400 sampling points with 1 s sampling interval. The first 80% samples of clock bias and pseudo-range are used as training data and validation data, and the last 20% samples are used as the true values of the predicted data for comparative analysis. This LSTM model is trained

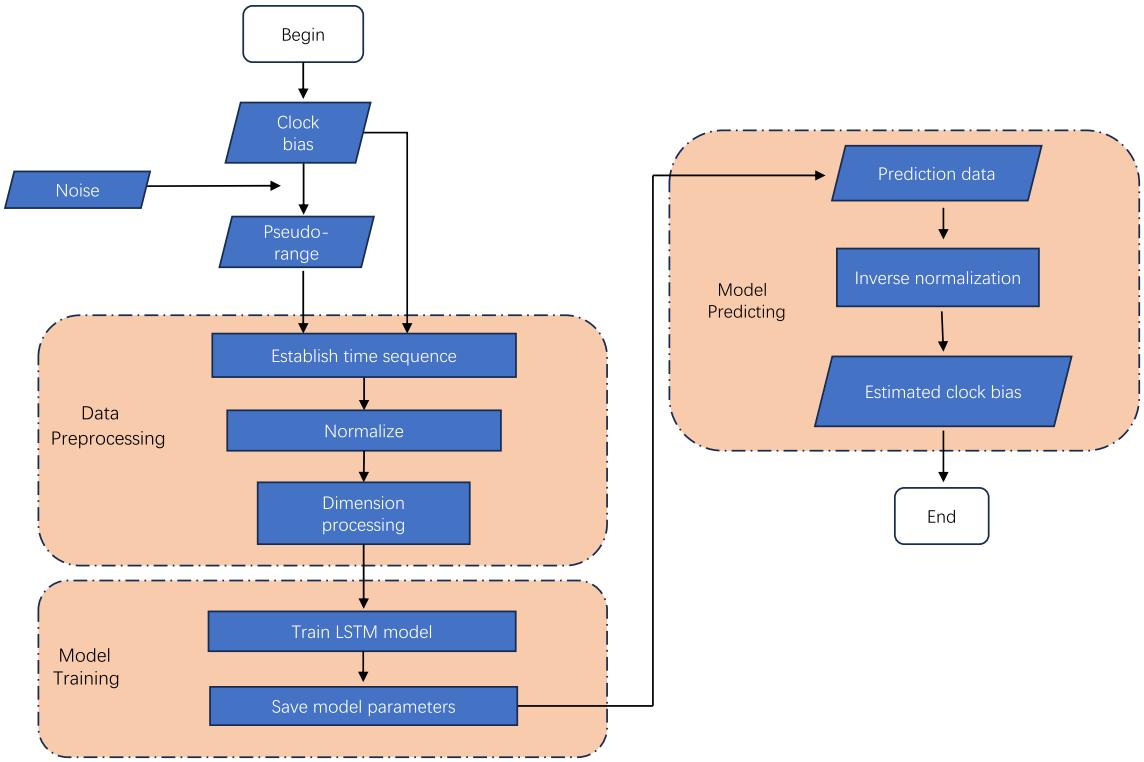


**Fig. 5** The flowchart of the proposed LSTM-based approach

**Table 1** List of the LSTM model parameters

| No | Parameter | Value |
|---|---|---|
| 1 | Number of LSTM layers | 1 layer (64 units) |
| 2 | Number of dense layers | 1 |
| 3 | Number of training epochs | 200 |
| 4 | Input dimension size | (200,2) |
| 5 | Output dimension size | 1 |
| 6 | Batch size | 100 |
| 7 | Learning rate | 0.01 |
| 8 | Validation data rate | 0.2 |
| 9 | Loss function | MSE |
| 10 | Optimizer | Adam |

by using Adam algorithm as the optimizer with learning rate of 0.01 (Kingma and Ba 2014). To analyze the optimal time-step in this scenario, we take the root mean square error (RMSE) result of different time-step lengths in the GRACE mission as an example for analysis. The RMSE is defined as follows:

$$\mathrm{RMSE} = \sqrt{\frac{1}{n}\sum_{k=1}^{n}(y_k - \hat{y}_k)^2} \tag{15}$$

where $\hat{y}_k$ and $y_k$ are the predicted and true values of satellite clock bias at sequence number $k$, respectively, and $n$ is the prediction times.

Figure 6 shows the RMSE of the estimated and true values with time-step from $t_s = 10$ to $t_s = 200$. The slight variations in results are caused by the randomness of the initial weights and bias values of neural network model. This variability is normal and fluctuates within a certain range. As shown in the shapes of boxes, the training results are less stable from $t_s = 10$ to $t_s = 120$, and they have more outliers. It indicates the model we proposed still can not capture the pattern of the data effectively. However, from $t_s = 120$ to $t_s = 200$, the RMSE becomes more stable and gradually converges with less outliers, which is able to provide a reference to the model parameter selection strategy. Although the increasing time-step can improve the accuracy, it also extends the training duration. Additionally, this analysis result also suggests that the increasing time-step has certain limitations on the model accuracy when $t_s \geq 120$. Based on the discussions above, for the sake of comprehensively considering training time and accuracy, we set $t_s = 200$ in this paper.

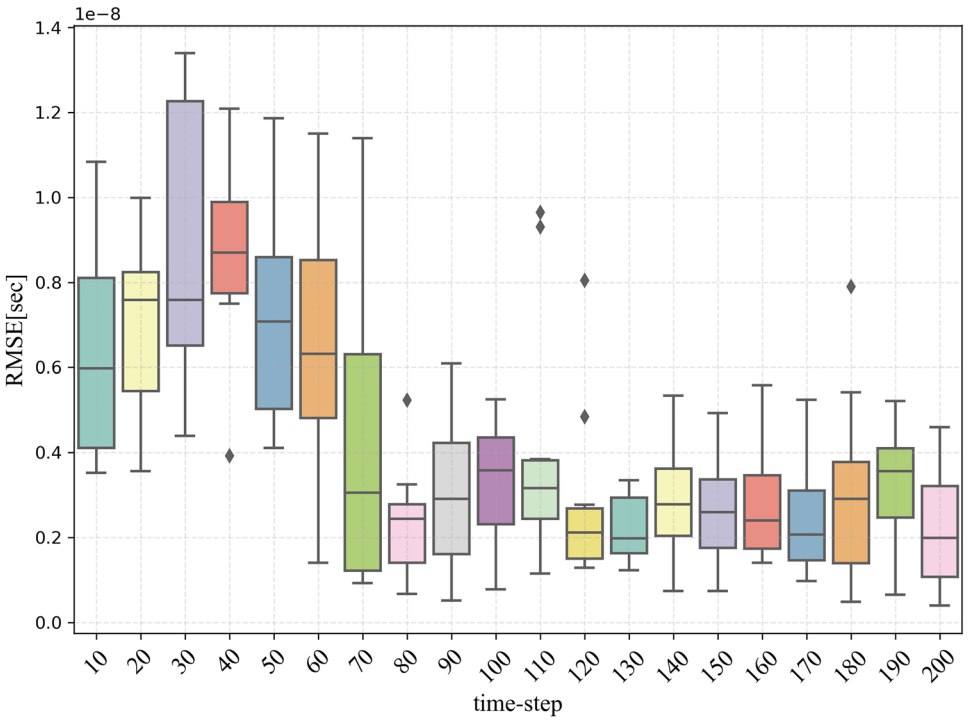


**Fig. 6** Box plot of the estimated and true values for varying time-step values

## Case studies

In this section, we evaluate and analyze the performance of the proposed method in the scenario of the GRACE mission. The original satellite data are obtained by the STK, which is capable of simulating satellite constellations. To get the pseudo-range measurement information, we regard the GRACE satellites motion over a day as the input of STWR model. After operation of data processing, we transform the pseudo-range measurements and clock bias into the input format of LSTM model in a ratio of 60% training data, 20% validation data, 20% test data. Without loss of generality, we let the phase deviation $a_0 = 1 \times 10^{-8}$ s, the frequency deviation $a_1 = 1 \times 10^{-12}$, and the frequency drift $a_2 = 1 \times 10^{-16}$ /s. As a comparison, we also present the estimation results under different clock stabilities. We set the speed of light $c = 3 \times 10^8$ m/s, and the Allan deviation (ADEV) of each phase noise component at $\tau = 1$ s is shown in Table 2.

### Effect of clock stability

First, we consider the impact of noise with different standard deviations on the estimation performance of the LSTM model. Let the time interval of STWR $\delta = 1$ s. Figures 7, 8, 9, 10, 11, 12, 13 and 14 depict the simulation results of the proposed LSTM estimator, the LS estimator proposed in (X. Gu et al. 2020) and the method based on the prior information (Xu et al. 2012), which are represented in red color, green color and blue color, respectively.

From Figs. 7, 8, 9 and 10, it is evident that on the test data, after converting pseudo-range data into the corresponding format and subsequently inverse normalization to be the input of LSTM model, we can obtain highly accurate clock bias data for the corresponding time instant, exhibiting a trend consistent with the original clock bias model. The residual value for this result is also presented in Figs. 7, 8, 9, 10b. By comparison, we note that the decoupling method based on the prior information outperforms the others due to the accurate position and velocity can be used to calculate the signal propagation time so that the clock bias can be decoupled accurately. But the proposed method achieves

**Table 2** ADEVs of four clocks with different stabilities

| Number | Designation | RWFM | FFM | WFM | FPM | WPM |
|---|---|---|---|---|---|---|
| 1 | $\sigma$ at $\tau = 1s$ | $1.2 \times 10^{-11}$ | $1.0 \times 10^{-10}$ | $1.0 \times 10^{-10}$ | $1.0 \times 10^{-9}$ | $1.0 \times 10^{-9}$ |
| 2 | $\sigma$ at $\tau = 1s$ | $1.2 \times 10^{-12}$ | $1.0 \times 10^{-11}$ | $1.0 \times 10^{-11}$ | $1.0 \times 10^{-10}$ | $1.0 \times 10^{-10}$ |
| 3 | $\sigma$ at $\tau = 1s$ | $1.2 \times 10^{-13}$ | $1.0 \times 10^{-12}$ | $1.0 \times 10^{-12}$ | $1.0 \times 10^{-11}$ | $1.0 \times 10^{-11}$ |
| 4 | $\sigma$ at $\tau = 1s$ | $1.2 \times 10^{-14}$ | $1.0 \times 10^{-13}$ | $1.0 \times 10^{-13}$ | $1.0 \times 10^{-12}$ | $1.0 \times 10^{-12}$ |

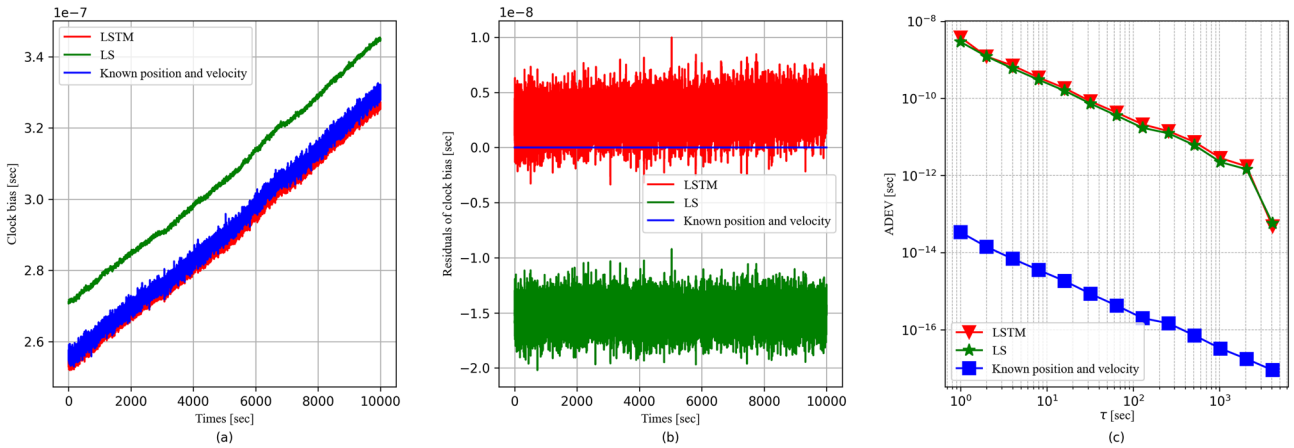


**Fig. 7** Comparison of the proposed method and existing methods using No.1 clock in Table 2 for $\delta = 1$ s. The results of **a** the estimated clock bias, **b** residual clock bias and **c** ADEVs of the residual clock bias are given, respectively

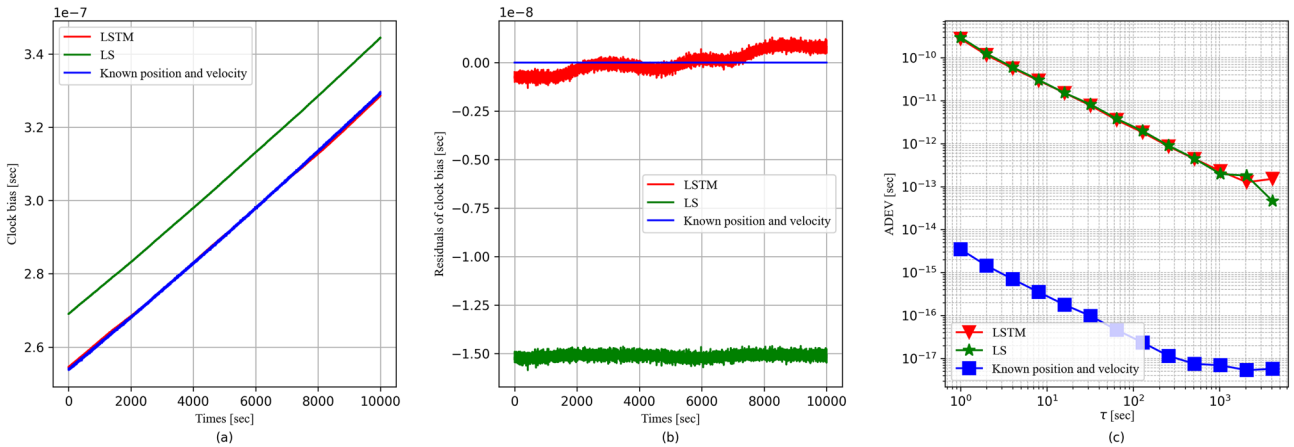


**Fig. 8** Comparison of the proposed method and existing methods using No.2 clock in Table 2 for $\delta = 1$ s. The results of **a** the estimated clock bias, **b** residual clock bias and **c** ADEVs of the residual clock bias are given, respectively

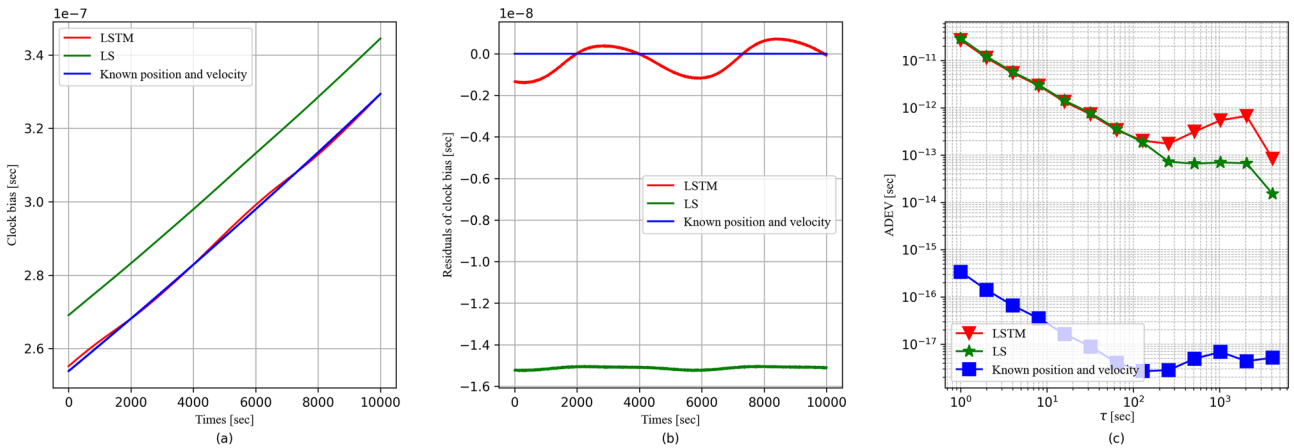


**Fig. 9** Comparison of the proposed method and existing methods using No.3 clock in Table 2 for $\delta = 1$ s. The results of **a** the estimated clock bias, **b** residual clock bias and **c** ADEVs of the residual clock bias are given, respectively

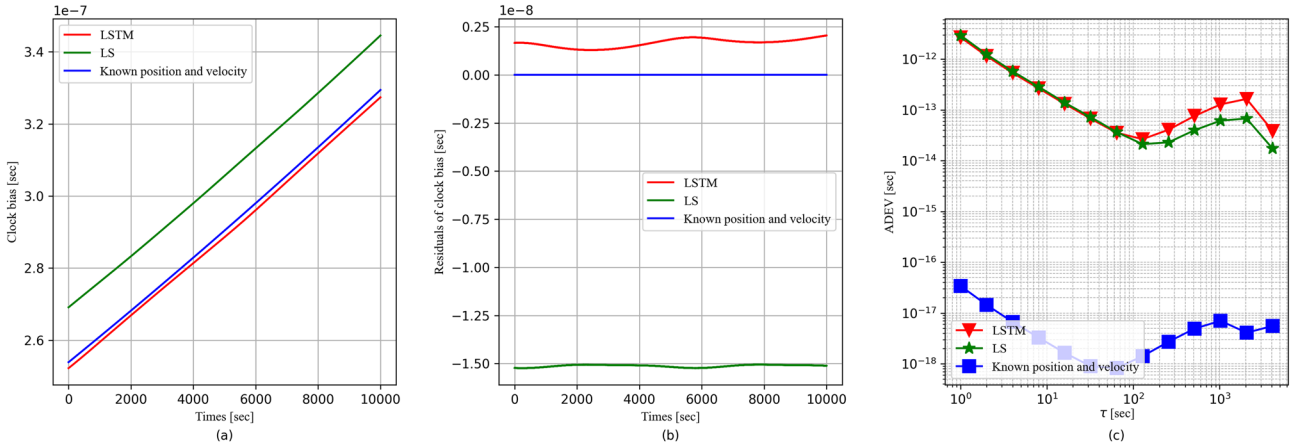


**Fig. 10** Comparison of the proposed method and existing methods using No.4 clock in Table 2 for $\delta = 1$ s. The results of **a** the estimated clock bias, **b** residual clock bias and **c** ADEVs of the residual clock bias are given, respectively

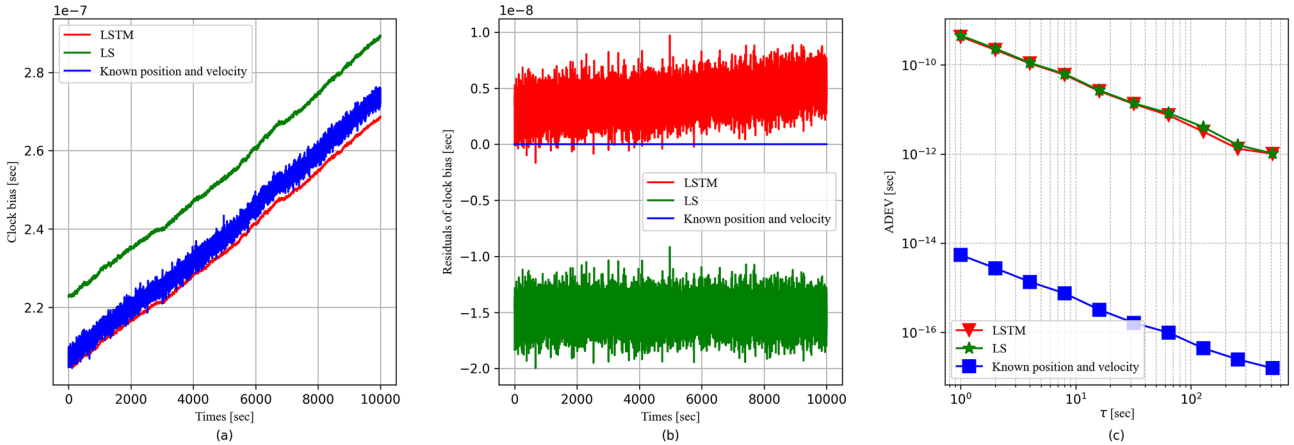


**Fig. 11** Comparison of the proposed method and existing methods using No.1 clock in Table 2 for $\delta = 0.2$ s. The results of **a** the estimated clock bias, **b** residual clock bias and **c** ADEVs of the residual clock bias are given, respectively

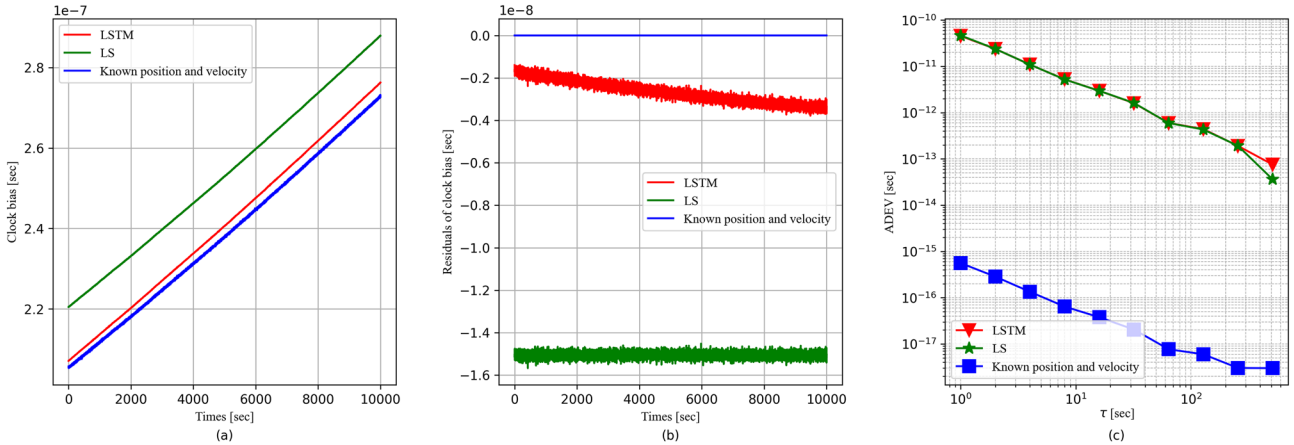


**Fig. 12** Comparison of the proposed method and existing methods using No.2 clock in Table 2 for $\delta = 0.2$ s. The results of **a** the estimated clock bias, **b** residual clock bias and **c** ADEVs of the residual clock bias are given, respectively

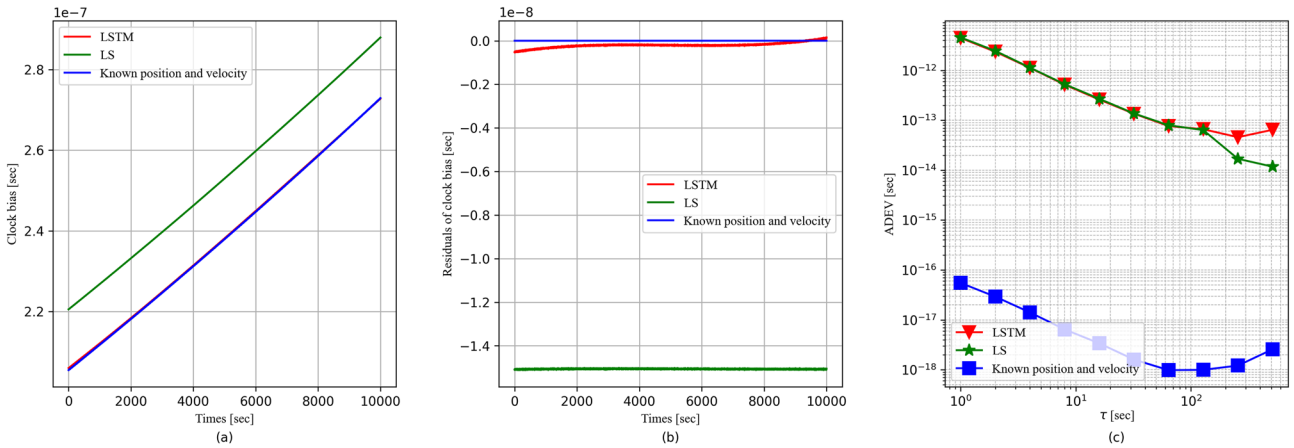


**Fig. 13** Comparison of the proposed method and existing methods using No.3 clock in Table 2 for $\delta = 0.2$ s. The results of **a** the estimated clock bias, **b** residual clock bias and **c** ADEVs of the residual clock bias are given, respectively

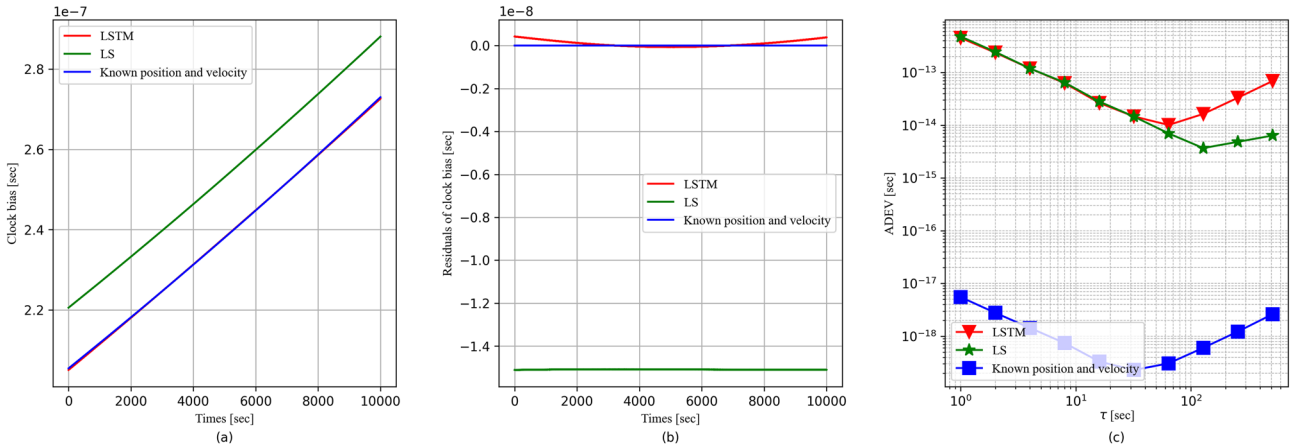


**Fig. 14** Comparison of the proposed method and existing methods using No.4 clock in Table 2 for $\delta = 0.2$ s. The results of **a** the estimated clock bias, **b** residual clock bias and **c** ADEVs of the residual clock bias are given, respectively

a better performance than the LS method in accuracy. In addition, it can be found that changing phase noise does not affect the actual effect of this model. It signifies that the LSTM model has effectively learned and fitted the relationship between pseudo-range and clock bias within the neural network during the training process with the absence of position and velocity information.

Observing Figs. 7, 8, 9, 10b, it can be found that the LSTM has an oscillation performance. The reason is that, for neural network algorithms, the residuals normally fluctuate instead of converging to a constant value. As the relative motion between satellites, the pseudo-range measurements change over time, the LSTM model has difficulty to perfectly capture all the slight changes but it still can achieve better accuracy than LS approach. On the other hand, the results shown in Figs. 7, 8, 9, 10c also indirectly describe this phenomenon. The long-term stability performance of the proposed method is slightly worse than LS owing to the oscillation.

## Effect of communication time interval

The corresponding clock bias estimation plots for varying clocks under time interval of communication $\delta = 0.2$ s are displayed in Figs. 11, 12, 13 and 14. The error plots illustrate the performance of the model by depicting the disparity between the estimated and true clock bias values. From the result we present, it can be found that the decreased communication time interval can enhance the performance of LSTM approach. When communication time interval $\delta = 0.2$ s, the proposed method achieves a better performance in estimation accuracy, signifying the correlation of data can be captured more efficiently in this case. As for the performance of stability, the shorter

communication time interval also improves the long-term stability, which is shown in Figures 7, 8, 9, 10, 11, 12, 13 and 14c. Therefore, both the accuracy and stability can be improved as the communication time interval decreases. However, the value of communication time interval cannot be set as small as possible, since the other factors such as power consumption, calculation time and complexity of the network topology must also be taken into account.

The random property and uncertainty of the data will lead to the fluctuation of residuals. According to Figures 7, 8, 9, 10, 11, 12, 13 and 14c, it can be found that when the noise component decreases, the degree of oscillation of residuals is reduced. In addition, in comparison to the results shown in Figs. 7, 8, 9, 10c for $\delta = 1$ s, the difference in long-term stability performance between the proposed method and the LS method becomes smaller. Therefore, we can infer that the communication time interval relates to the accuracy and stability performances of the proposed method.

Moreover, according to Figures 7, 8, 9, 10, 11, 12, 13 and 14b, it can be seen that the varying communication time interval also have different effects on the estimation accuracy of the LSTM and LS. As the communication time interval decreases, the deviation of LS is always stable at around $1.5 \times 10^{-8}$ s, while the estimation accuracy of LSTM improves significantly. The reason is that the LS is a batch filter, changing communication time interval results in a narrower time window, if the size of the input data does not change. In this case, the fitting performance of the ranging coefficient to the relative motion state determines the estimation accuracy.

## LSTM model evaluation

The experimental results are summarized in Figs. 15(a), (b) and 16, which provide a comprehensive comparison of RMSE for the neural network models established for the GRACE mission satellite system under varying levels of phase noise and time interval of communication in the clock bias models. Figure 15(a) and (b) offer valuable insights into the performance of our neural network models across different noise scenarios,

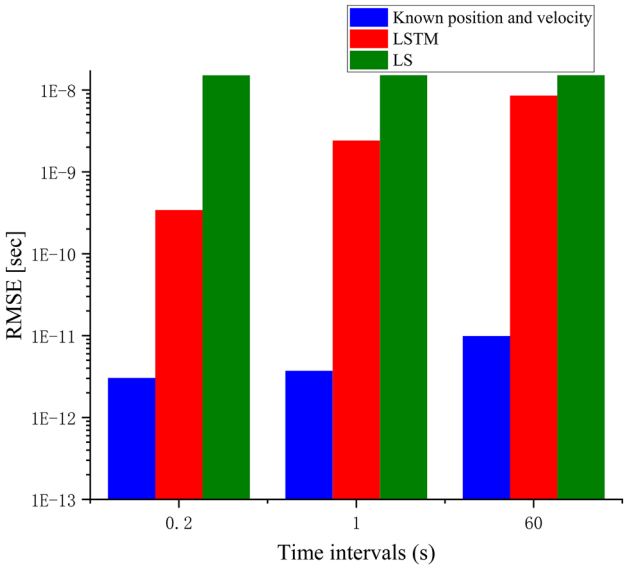


**Fig. 16** RMSEs of the proposed method and existing estimators for communication time intervals $\delta$ of 0.2 s, 1 s, 60 s using No.4 clock

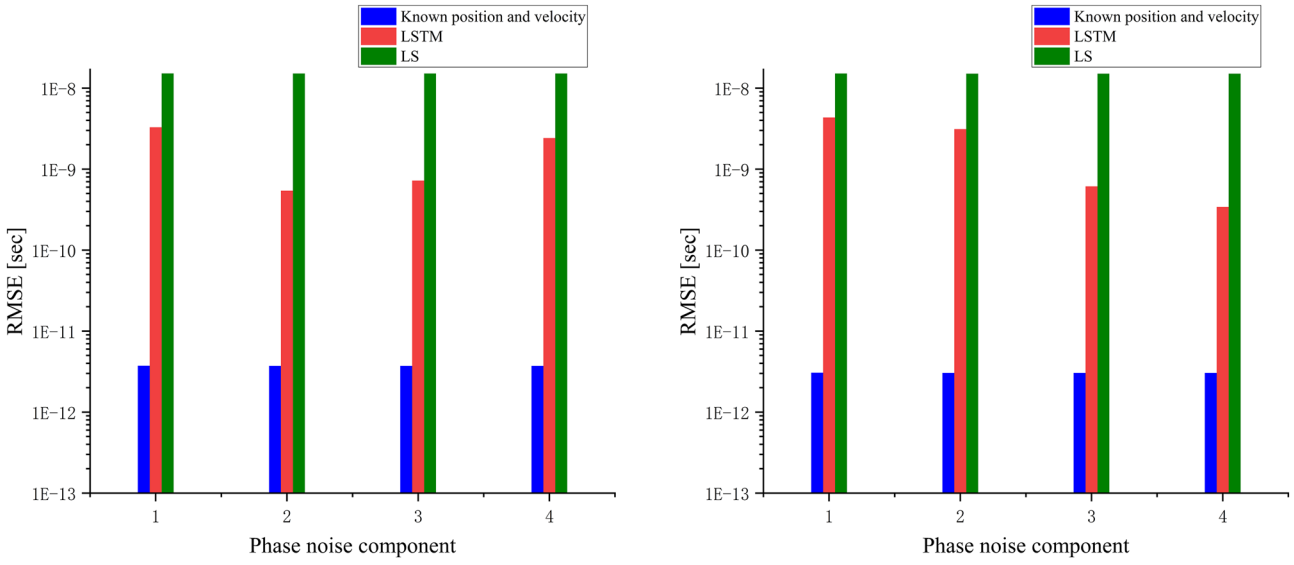


**Fig. 15** **a**: RMSEs[sec] for different on-board clocks with communication time interval $\delta = 1$ s. **b**: RMSEs[sec] for different on-board clocks with communication time interval $\delta = 0.2$ s

allowing us to assess their robustness and accuracy in handling variations in phase noise and time interval of communication. As we can see from Fig. 16, with the increase in time interval of communication, there is a tendency for a reduction in effective information on the time sequence. This will impact the performance of the LSTM clock bias estimation model. In the context of satellite motion, when the time interval of communication reaches 60 s, significant variations in satellite information become apparent. Despite this challenge, the accuracy of this estimator remains an order of magnitude higher than that of the LS estimator.

Since the model is built on the relationship between pseudo-range variations and clock bias trends, it becomes particularly useful when satellites lose continuous and precise information support regarding their orbits and velocities. Therefore, when the master satellite and slave satellites perform clock synchronization via STWR, the proposed approach provide a novel aspect to decouple the clock error frrom pseudo-range measurements without modelling the non-linear relativc motion, which results in a higher accuracy compared with the LS-based approach.

## Conclusion

In this paper, a LSTM-based parameter estimation method was proposed to solve the satellite clock synchronization problem using ISL ranging measurements. We investigated the LSTM-based estimation method based on STWR ranging measurements under various clock models and communication time intervals. Simulation results indicate that the proposed LSTM-based approach achieves a very close performance to the algorithm which utilizes ephemeris data, and outperforms existing clock bias estimation algorithms which use pseudo-range measurements or exchanged timing tags. The proposed approach can also be applied in other networks with unsynchronized clocks and limited observable measurements. Future work may include dealing with the problem of clock synchronization under partial one-way ranging measurements in complex environments.

**Acknowledgements** This work was supported in part by the National Natural Science Foundation of China under Grant 62101138; in part by the Natural Science Foundation of Guangdong Province under Grant 2022A1515012573; and in part by the Scientific and Technological Planning Project of Guangzhou City under Grant 2024A04J9894.

**Author contributions** GX, QZ contributed to conceptualization; GX, WY, JW contributed to methodology; GX, QZ done formal analysis, investigation, and writing—original draft preparation; WY, JW helped in writing—review and editing.

**Funding** This work was supported in part by the National Natural Science Foundation of China under Grant 62101138; in part by the Natural Science Foundation of Guangdong Province under Grant 2022A1515012573; and in part by the Scientific and Technological Planning Project of Guangzhou City under Grant 2024A04J9894.

**Data availability** Not applicable.

## Declarations

**Conflict of interest** The authors declare that they have no known competing financial interests or personal relationships that could have appeared to influence the work reported in this paper.

**Consent for publication** Not applicable.

**Consent to participate** Not applicable.

**Ethical approval**
Not applicable.

### References

Allan DW, Gray JE, Machlan HE (1972) The national bureau of standards atomic time scales: generation, dissemination, stability, and accuracy. IEEE Trans Instrum Meas 21(4):388–391. https://doi.org/10.1109/TIM.1972.4314051

Domuta I, Palade TP (2021) Two-Way Ranging Algorithms for Clock Error Compensation. IEEE Trans Veh Technol 70(8):8237–8250. https://doi.org/10.1109/TVT.2021.3096667

Fernandez-Hernandez I, Chamorro-Moreno A, Cancela-Diaz S, Calle-Calle JD, Zoccarato P, Blonski D et al (2022) Galileo high accuracy service: initial definition and performance. GPS Solut 26(3):65. https://doi.org/10.1007/s10291-022-01247-x

Fujieda M, Piester D, Gotoh T, Becker J, Aida M, Bauch A (2014) Carrier-phase two-way satellite frequency transfer over a very long baseline. Metrologia 51(3):253. https://doi.org/10.1088/0026-1394/51/3/253

Glennon E, Gauthier J, Choudhury M, Dempster A, Parkinson K (2013) 'Synchronization and syntonization of formation flying cubesats using the namuru V3. In: 2 spaceborne GPS receiver' Proceedings of the ION 2013 Pacific PNT Meeting. pp. 588–597.

Gu X, Chang Q, Glennon EP, Xu B, Dempster AG, Wang D et al (2015) An autonomous satellite time synchronization system using remotely disciplined VC-OCXOs. Sensors 15(8):17895–17915. https://doi.org/10.3390/s150817895

Gu X, Zhou G, Li J, Xie S (2020) Joint time synchronization and ranging for a mobile wireless network. IEEE Commun Lett 24(10):2363–2366. https://doi.org/10.1109/LCOMM.2020.3001138

Gu X, Li J, Zhou G, Xie S (2021) Improved clock parameters tracking and ranging method based on two-way timing stamps exchange mechanism. IEEE Signal Process Lett 28:598–602. https://doi.org/10.1109/LSP.2021.3062483

Haidar-Ahmad J, Khairallah N, Kassas ZM (2022). A hybrid analytical-machine learning approach for LEO satellite orbit prediction. In: 022 25th International Conference on Information Fusion (FUSION) (pp. 1-7). IEEE.

He S, Liu J, Zhu X, Dai Z, Li D (2023) Research on modeling and predicting of BDS-3 satellite clock bias using the LSTM neural network model. GPS Solut 27(3):108. https://doi.org/10.1007/s10291-023-01451-3

Huang B, Ji Z, Zhai R, Xiao C, Yang F, Yang B et al (2021) Clock bias prediction algorithm for navigation satellites based on a supervised learning long short-term memory neural network. GPS Solut 25(2):80. https://doi.org/10.1007/s10291-021-01115-0

Iwata T, Machita K, Matsuzawa T (2010). Actual operation simulation of RESSOX ground experiments. In: Proceedings of the 42nd

Annual Precise Time and Time Interval Systems and Applications Meeting (pp. 141-160).
Kai X, Chunling W, Liangdong L (2013) Autonomous navigation for a group of satellites with star sensors and inter-satellite links. Acta Astro 86:10–23. https://doi.org/10.1016/j.actaastro.2012.12.001
Karthik AK, Blum RS (2020) Robust clock skew and offset estimation for IEEE 1588 in the presence of unexpected deterministic path delay asymmetries. IEEE Trans Commun 68(8):5102–5119. https://doi.org/10.1109/TCOMM.2020.2991212
Kim J, Tapley BD (2003) Simulation of dual one-way ranging measurements. J Spacecr Rocket 40:419–425. https://doi.org/10.2514/2.3962
Kingma DP, Ba J (2014). Adam: a method for stochastic optimization, Corr, https://doi.org/10.48550/arXiv.1412.6980.
Lipton ZC (2015). A critical review of recurrent neural networks for sequence learning. ArXiv, abs/1506.00019. https://doi.org/10.48550/arXiv.1506.00019.
Meng Y, Lei W, Bian L, Yan T, Wang Y (2020) Clock tuning technique for a disciplined high medium–long-stability GNSS oscillator with precise clock drifts for LEO users. GPS Solutions 24(4):110. https://doi.org/10.1007/s10291-020-01025-7
Michalak G, Glaser S, Neumayer KH, König R (2021) Precise orbit and Earth parameter determination supported by LEO satellites, inter-satellite links and synchronized clocks of a future GNSS. Adv Space Res 68(12):4753–4782. https://doi.org/10.1016/j.asr.2021.03.008
Powers E, Colina A (2016) Wide area wireless network synchronization using Locata. In: Proceedings of the 47th Annual Precise Time and Time Interval Systems and Applications Meeting. pp. 90–98. https://doi.org/10.33012/2016.13152.
Rajan RT, van der Veen AJ (2015) Joint ranging and synchronization for an anchorless network of mobile nodes. IEEE Trans Sig Process 63(8):1925–1940. https://doi.org/10.1109/TSP.2015.2391076
Ruan R, Jia X, Feng L, Zhu J, Huyan Z, Li J et al (2020) Orbit determination and time synchronization for BDS-3 satellites with raw inter-satellite link ranging observations. Sat Navigat 1(1):8. https://doi.org/10.1186/s43020-020-0008-y
Sherstinsky A (2020) Fundamentals of recurrent neural network (RNN) and long short-term memory (LSTM) network. Phys D: Nonlinear Phenomena 404:132306. https://doi.org/10.1016/j.physd.2019.132306
Wang Y, Lu Z, Qu Y, Li L, Wang N (2017) Improving prediction performance of GPS satellite clock bias based on wavelet neural network. GPS Solutions 21(2):523–534. https://doi.org/10.1007/s10291-016-0543-z
Xie X, Geng T, Zhao Q, Lv Y, Cai H, Liu J (2020) Orbit and clock analysis of BDS-3 satellites using inter-satellite link observations. J Geodesy 94(7):64. https://doi.org/10.1007/s00190-020-01394-4
Xu Y, Chang Q, Yu Z (2012) On new measurement and communication techniques of GNSS inter-satellite links. SCIENCE CHINA Technol Sci 55(1):285–294. https://doi.org/10.1007/s11431-011-4586-7
Ya S, Zhao X, Liu C, Chen J, Liu C, Hu H (2022) Enhancing short-term prediction of BDS-3 satellite clock bias based with BSO optimized BP neural network. Int J Aerospace Eng. https://doi.org/10.1155/2022/8435033

**Publisher's Note** Springer Nature remains neutral with regard to jurisdictional claims in published maps and institutional affiliations.

Springer Nature or its licensor (e.g. a society or other partner) holds exclusive rights to this article under a publishing agreement with the author(s) or other rightsholder(s); author self-archiving of the accepted manuscript version of this article is solely governed by the terms of such publishing agreement and applicable law.

**Xiaobo Gu** received the B.Eng. and M.Sc. degrees from The University of Electronic Science and Technology of China, Chengdu, China, in 2008 and 2011, respectively, and the Ph.D. degree from Beihang University, Beijing, China, in 2016. He is currently an Associate Professor with the School of Integrated Circuits, Guangdong University of Technology, Guangzhou, China. From 2016 to 2018, he was the Director of the Power Dispatching and Control Center, China Southern Power Grid, Guangzhou, China. His research interests include signal processing and communication systems, particularly synchronization, ranging and positioning techniques for wireless networks.

**Zeyang Qiu** received the B.E. degree from School of Electrical Engineering and Intelligentization, Dongguan University of Technology, Dongguan, China, in 2021. He is currently a M.E candidate of Control Engineering with the School of Automation, Guangdong University of Technology, Guangzhou China. His research interests include deep learning and satellite navigation.

**Yanjiao Wang** was born in Donghai, Jiangsu Province, China. She received the Ph.D. degree from the Jiangnan University (Wuxi, China) in 2019. She is currently a lecturer with the School of Automation, Guangdong University of Technology, Guangzhou. Her interests include system modeling, system identification and signal processing.

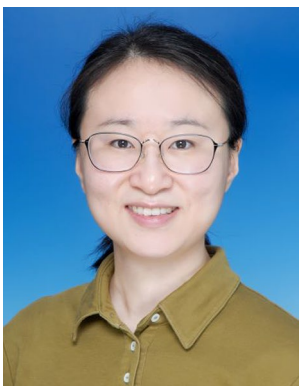

**Wei Jiang** is Professor at the School of Automation and Intelligence, Beijing Jiaotong University. She received her PhD degree from the School of Civil & Environmental Engineering, University of New South Wales (UNSW), Sydney, Australia. Her current research interest is multi-sensor integration, and in particular the implementation of new navigation and data fusion algorithms.